Title: Loss of Tousled-Like Kinase 2 Reduces Antioxidative Responses and Disrupts Brain Development

Qiannan Deng[1,*], Fanjia Hou[2,*], Xiaoqi Zhou[3], Yiwen Zhang[4], Qing Zhang[2], Jiaqi Zhang[5,6], Zihan Zhang[2,7], Tongfei Liu[5,6], Wen Yuan[1,2,8], Chaochun Zou[4], Chao Tong[3,9], Ke Zhang[1,2,8, #]

[1] Rare Disease Center, Shenzhen Medical Academy of Research and Translation, Shenzhen, Guangdong 518107, China, P.R.

[2] Institute of Neurological and Psychiatric Disorders, Shenzhen Bay Laboratory, Shenzhen, Guangdong 518107, China, P.R.

[3] MOE Key Laboratory for Biosystems Homeostasis & Protection and Innovation Center for Cell Signaling Network, Life Sciences Institute, Zhejiang University, Hangzhou, Zhejiang 310058, China, P.R.

[4] Department of Endocrinology, Children's Hospital, Zhejiang University School of Medicine, National Clinical Research Center for Child Health, Hangzhou, Zhejiang 310052, China, P.R.

[5] Department of Neurology, The First Affiliated Hospital of Chongqing Medical University, Chongqing 400016, China, P.R.

[6] Department of Neurology, School of Basic Medical Sciences, Key Laboratory of Major Brain Disease and Aging Research (Ministry of Education), Chongqing Medical University, Chongqing 400016, China, P.R.

[7] National Engineering Laboratory for AIDS Vaccine, School of Life Sciences, Jilin University, Changchun130012, China，P.R.

[8] Ph.D. Program, Shenzhen Medical Academy of Research and Translation, Shenzhen,

Guangdong 518107, China, P.R.

[9] The Second Affiliated Hospital, School of Medicine, Zhejiang University, Hangzhou, Zhejiang 310009, China, P.R.

* Contribute equally

Correspondence to:

Ke Zhang, Institute of Neurological and Psychiatric Disorders, Shenzhen Bay Laboratory, Shenzhen, Guangdong, 518107, China, P.R. Email: ke.zhang@szbl.ac.cn,

Highlights

Tlk loss disrupts neural stem cell differentiation and causes microcephaly in *Drosophila*.

Tlk loss causes oxidative stress by suppressing the Nrf2-mediated antioxidative responses.

TLK2 loss downregulates ATF4 and Nrf2, increases oxidative stress, and causes microcephaly in patient brain organoids.

ABSTRACT

Haploinsufficiency of tousled-like kinase 2 (TLK2) causes intellectual developmental disorder, autosomal dominant 57, a rare neurodevelopmental disorder with unclear pathomechanism and no effective treatment. Here, we established *Drosophila* models with neurodevelopmental defects resembling some disease features, such as microcephaly. Further studies suggested that oxidative stress plays a critical role in these models. Mechanistically, Tlk (the fly homolog of TLK2) loss reduces the expression of antioxidative genes via activating transcription factor 4 (ATF4) and its downstream protein, nuclear factor erythroid 2-related factor 2 (Nrf2), a transcriptional activator of antioxidative genes, in fly neural stem cells (NSCs), thereby disrupting NSC differentiation and causing microcephaly. In patient-derived brain organoids, ATF4, Nrf2, and their downstream antioxidative genes are also downregulated. Agreeing with these data, these organoids exhibited oxidative stress and microcephaly. Combined, our findings suggest that ATF4/Nrf2-mediated antioxidative stress responses play a critical role in TLK2-related disease and may be a therapeutic target.

Keywords: TLK2, rare neurodevelopmental disorder, microcephaly, oxidative stress

INTRODUCTION

Intellectual developmental disorder, autosomal dominant 57 (a.k.a. mental retardation, autosomal dominant 57, or MRD57) is a rare developmental disorder caused by heterozygous loss-of-function (LoF) mutations in *tousled-like kinase 2* (*TLK2*) (Reijnders, Miller et al. 2018). Less than 100 MRD57 patients have been reported, most of whom presented with microcephaly, epilepsy, delayed psychomotor development, and behavioral abnormalities during infancy or childhood. Some patients also presented with hypotonia, gastrointestinal issues, dysmorphic facial features, etc. (Reijnders, Miller et al. 2018, Pavinato, Villamor-Payà et al. 2022). Currently, there is no effective treatment.

TLK2 is an evolutionarily conserved kinase enriched in the brain. It plays roles in multiple cellular processes, such as cell cycle progression and chromosomal stability (Bruinsma, van den Berg et al. 2016, Lee, Segura-Bayona et al. 2018, Segura-Bayona and Stracker 2019). However, how its LoF causes a neurological disorder is unclear.

Mammals have two TLKs, TLK1 and TLK2 (Segura-Bayona, Knobel et al. 2017). TLK1 knockout (KO) mice showed no obvious phenotype, whereas TLK2 KO mice are embryonic lethal due to placental failure. Furthermore, TLK2 heterozygous KO or conditional KO after development causes no obvious phenotype in mice (Segura-Bayona et al., 2017). Hence, these mouse models do not mimic neurological conditions in MRD57 patients.

Here, we established *Drosophila* models with Tlk (the only TLK1/2 homolog in flies) LoF mutations. These flies are pupal lethal and exhibit patient-like phenotypes. Mechanistic studies suggested that Tlk LoF downregulates antioxidative genes via the activating transcription factor 4 (ATF4)/nuclear factor erythroid 2-related factor 2 (Nrf2) axis, causing oxidative stress and disrupted neural stem cell (NSC) differentiation. Upregulating ATF4 or Nrf2 mitigates oxidative stress and NSC defects, ameliorates

microcephaly, and suppresses lethality. Consistent with these data, brain organoids derived from an MRD57 patient exhibited growth defects, downregulated Nrf2, and elevated oxidative stress, suggesting that oxidative stress can be a critical pathogenic contributor in MRD57.

RESULTS

Tlk LoF causes neurodevelopmental defects in flies

We obtained a fly line with an intronic *P*-element insertion in *Tlk* (Tlk^{G0054}, Figure 1A). The *Tlk* mRNA level in hemizygous mutant larvae is reduced to ~40% of the wild-type control (Figure S1A). We also used CRISPR/Cas9 to generate a *Tlk* KO allele, Tlk^{1-12}, which has part of the second exon deleted, causing a frame shift and premature termination of translation (Figure 1A). The Tlk protein levels in hemizygous mutant larvae are reduced to ~30% of the wild-type control (Figure S1B and C), suggesting Tlk LoF. Both Tlk^{G0054} and Tlk^{1-12} cause pupal lethality when hemizygous (Figure 1B). A transgene containing the *Tlk* genomic region (referred to as Tlk duplication, or Tlk Dp) restores both mRNA and protein levels of Tlk (Figure S1A-C) and rescues the lethality in both alleles (Figure 1B), confirming that *Tlk* is essential.

To correlate our fly models with MRD57, we assessed the effects of Tlk LoF on development. Compared with the wild-type control, mutant larvae are smaller (Figure 1C and D) and require 2-3 more days to become pupae, suggesting a developmental delay. Additionally, their brains are smaller (Figures 1E and F), suggesting microcephaly. All these phenotypes were all fully rescued by Tlk Dp (Figure 1C-F), confirming that Tlk LoF causes neurodevelopmental defects mirroring patient features.

Figure 1

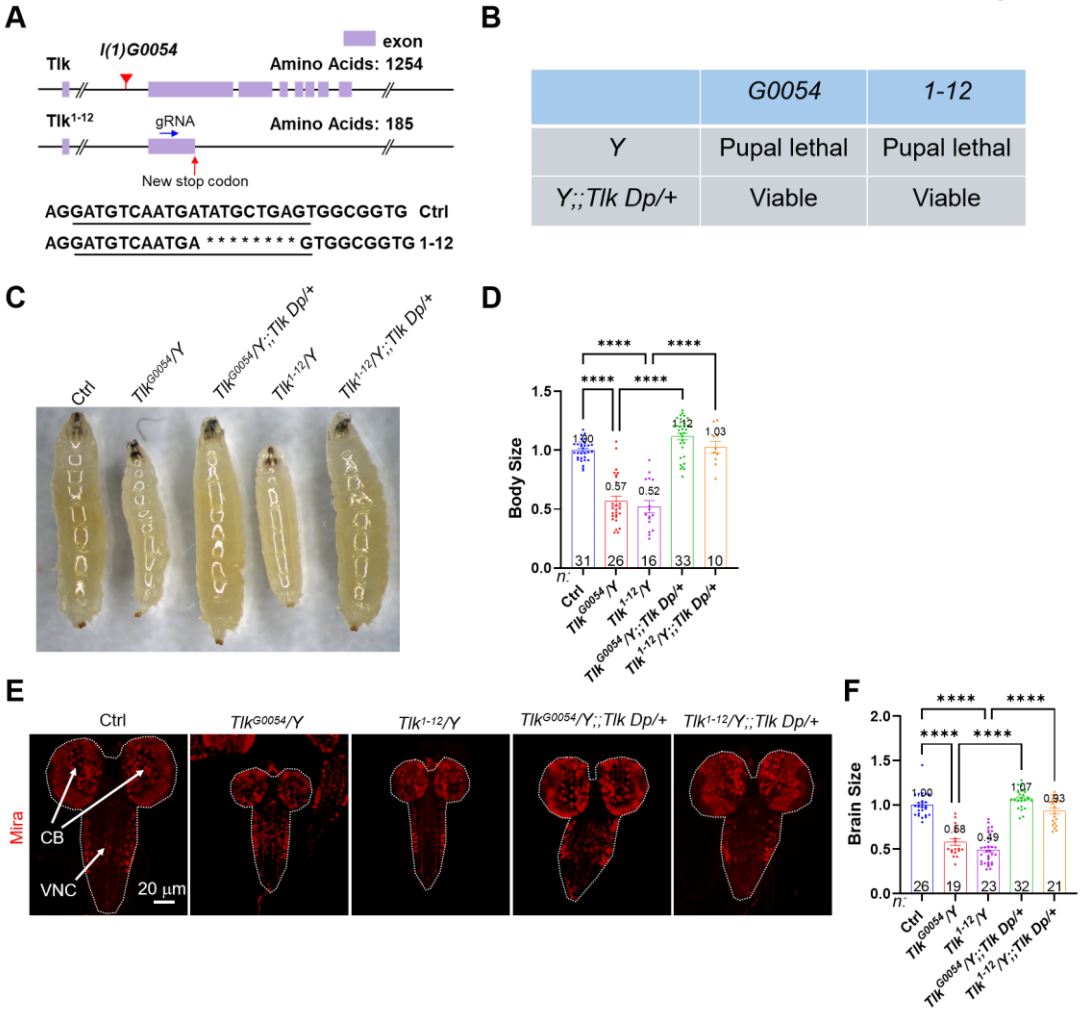

Figure 1. Tlk LoF causes neurodevelopmental defects in flies

(A) *Tlk* mutant alleles. (B) Lethal stages of *Tlk* alleles and rescue. (C) Images of third instar larvae. Ctrl, control. Larval body sizes were quantified in D. (E) Central nervous systems of third instar larvae were stained with Miranda (Mira, red). Brain sizes were quantified in F. Means ± SEM. One-way ANOVA with Tukey's tests. ****$p < 0.0001$.

Tlk LoF disrupts the asymmetric division of NSCs

Microcephaly is usually due to insufficient nerve cells, which can be caused by NSC defects. The Fly Cell Atlas database showed that Tlk is expressed in NSCs, as indicated by the NSC marker Deadpan (Dpn, Figure S1D). To test whether Tlk in NSCs plays a role in neurodevelopment, we expressed Tlk RNAi using the NSC-specific *inscutable* (*insc*)-GAL4. As shown in Figure S1E, two independent *Tlk* RNAi lines reduced larval brain size by ~60% and 30%, respectively, suggesting that Tlk LoF in NSCs causes microcephaly.

NSCs can proliferate or differentiate, the latter generating neurons and glia (Wang et al., 2009; Gateff and Schneiderman, 1974). Using a Dpn antibody, our immunofluorescent staining experiments showed that the total quantity of NSCs was unchanged in Tlk mutant larvae compared to the control (Figures S1F and G), suggesting that the NSC proliferation is unaffected.

Next, we assessed NSC differentiation, during which an NSC undergoes asymmetric division to generate a new NSC and a neural progenitor cell, the latter further differentiates into a neuron or glia (Doe 2008). We immunofluorescently stained polarity proteins, a group of asymmetrically localized proteins that establish the apicobasal polarity during the asymmetric division of NSCs. As shown in Figure 2A and B, the polarity proteins atypical protein kinase C (aPKC) and Miranda (Mira) are normally localized to the apical and basal cortex of NSCs, respectively, at metaphase. In NSCs of both G0054 and 1-12 alleles, they are mislocalized, which can be rescued by Tlk Dp. Additional apical polarity proteins, Bazooka (Baz) and Partitioning-defective protein 6 (Par6), are also mislocalized or missing in mutant NSCs (Figures S2A-D). Notably, Tlk LoF does not alter mRNA levels of these polarity proteins (Figure S2E) or disrupt the alignment of mitotic spindles (Figures S2F and G), which are essential for asymmetric division (Siller and Doe 2009). In summary, Tlk LoF disrupts NSC polarity,

which is essential to NSC differentiation.

Figure S1

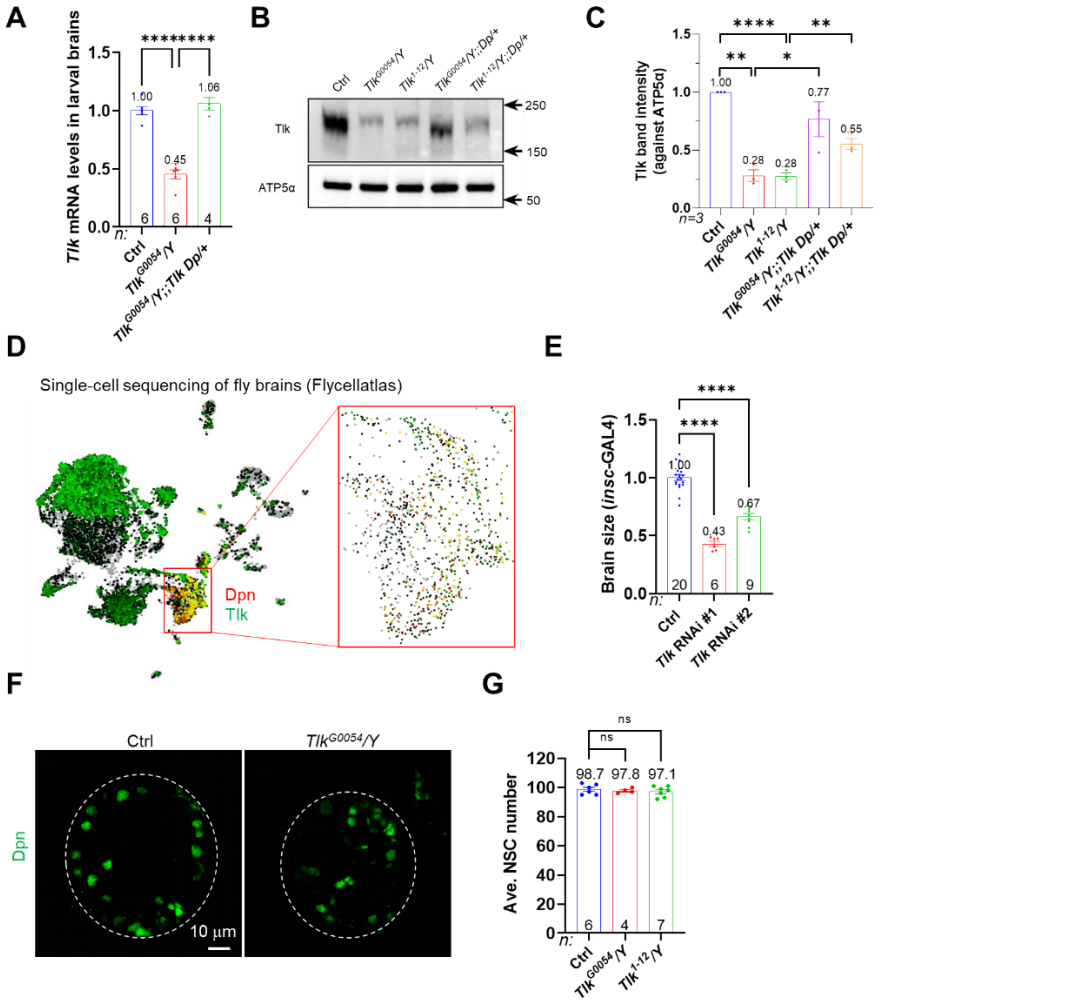

Figure S1. Tlk LoF does not affect NSC proliferation

(A) *Tlk* mRNA levels in third instar larval brains were measured by RT-PCR. Ctrl, control. (B) Western blots of larval brain extracts, quantified in C. (D) Re-analyses of the single-cell sequencing results of fly larval brains from Fly Cell Atlas, Tlk (green) and Dpn (red)-expressing cells were labeled. (E) Quantified brain sizes of larvae expressing *Tlk* RNAi in NSCs under the control of *insc*-GAL4. (F) Brain lobes of Ctrl or Tlk mutant third instar larvae were stained with Dpn (green). NSC numbers were quantified in G. Means ± SEM. One-way ANOVA with Dunnett's (A, E, and G) or Tukey's (C) tests. ns, not significant, *$p < 0.05$, **$p < 0.01$, ****$p < 0.0001$.

Figure 2

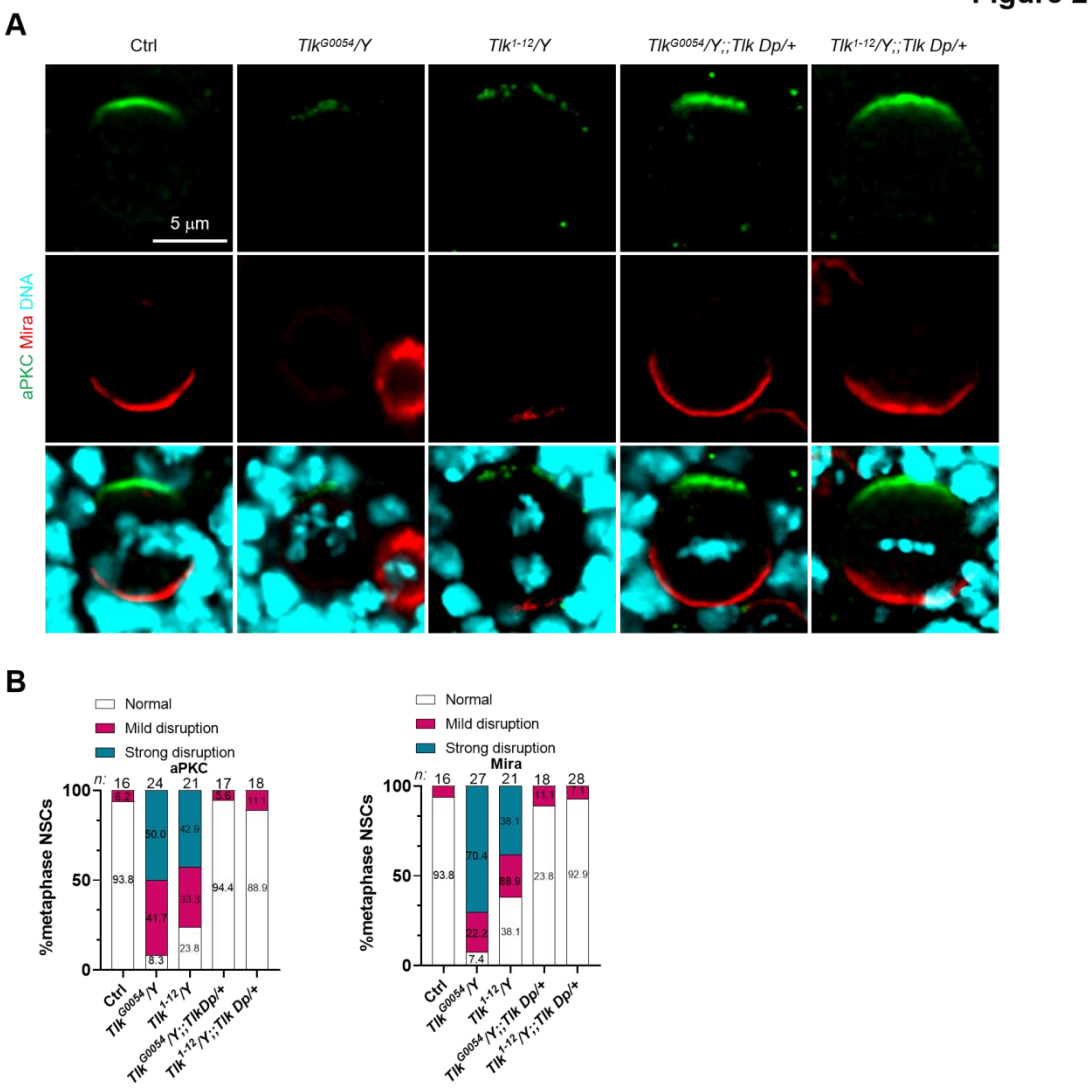

Figure 2. Tlk LoF disrupts NSC polarity

(A) Metaphase NSCs of larvae co-stained with aPKC (green), Mira (red), and DAPI (cyan, indicating DNA), quantified in B. Ctrl, control.

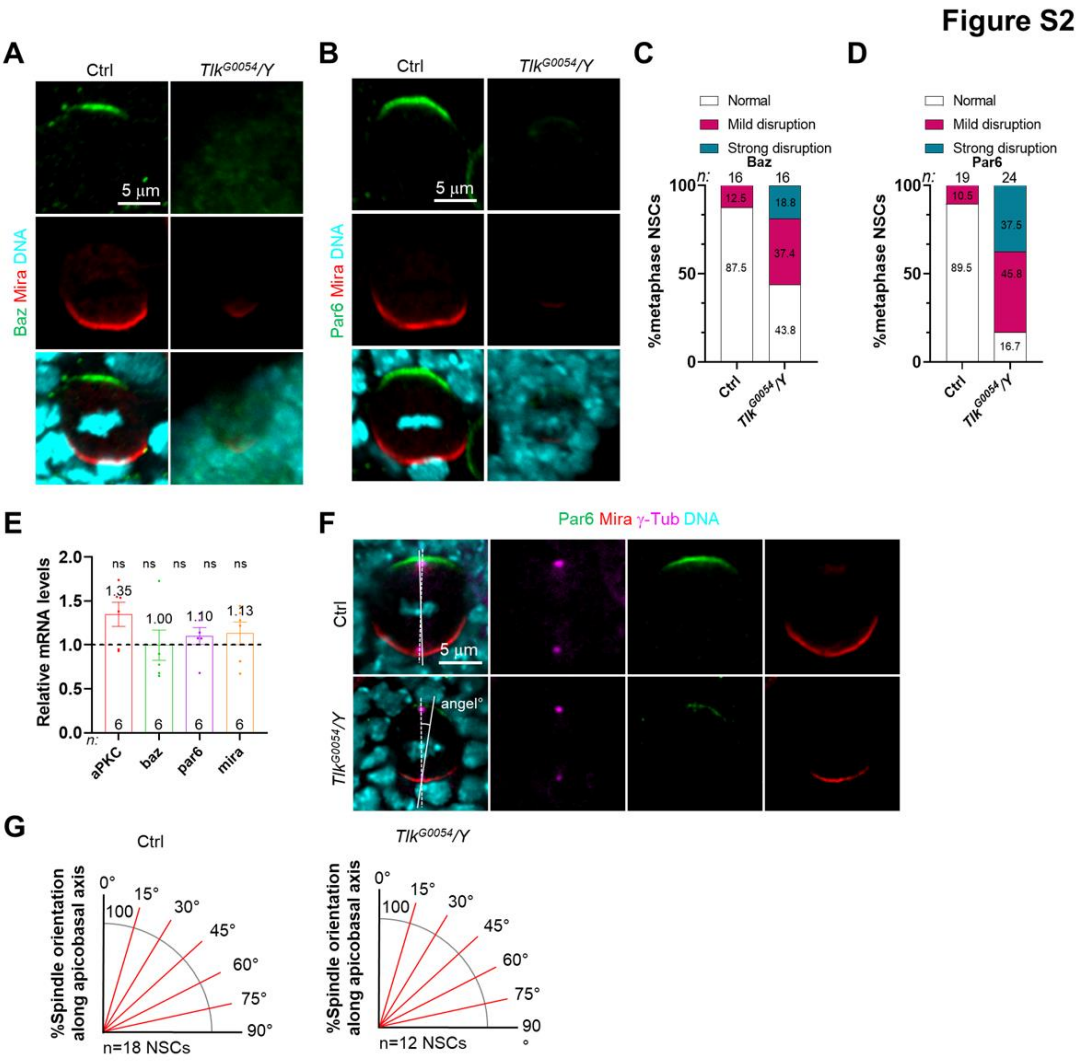

Figure S2. Tlk in NSCs is required for neurodevelopment

(A and B) Metaphase NSCs of larvae co-stained with Baz (A) or Par6 (B, green), Mira (red), and DNA (cyan), quantified in C and D. Ctrl, control. (E) RT-PCR results of t*aPKC*, *Mira*, *baz*, and *par6* in *Tlk*^{G0054}*/Y* larval brains, normalized to Ctrl. (F) Metaphase NSCs of larvae co-stained with Par6 (green), Mira (red), γ-Tub (magenta), and DNA (cyan). % spindle orientation along the apicobasal axis is allocated to a range of 0° to 90°, quantified in G. Mean ± SEM. Student's *t*-tests. ns, not significant.

Tlk LoF causes oxidative stress

Next, we sought to dissect the molecular mechanism by which Tlk LoF causes cytotoxicity. Previously, we performed an RNAi screen to identify genes regulating mitochondrial morphology, from which we identified that *Tlk* RNAi disrupts mitochondrial morphology in larval fat tissues (Zhou, Xu et al. 2019). Using a mitochondrially localized GFP (mitoGFP, a mitochondrial marker), we verified these data, as *Tlk* RNAi caused mitochondria to exhibit a non-tubular, either spotted or circular, shape (Figures S3A and B). Using MitoTracker staining, morphological defects were also observed in mitochondria in *Tlk* mutant NSCs, which are rescued by Tlk Dp (Figures 3A and B). Furthermore, TOM20 (a mitochondrial marker) staining showed that *TLK2* RNAi also caused morphological defects in HeLa cell mitochondria (Figures 3C and D). Combined, these data suggested that Tlk/TLK2 LoF disrupts mitochondrial morphology in fly fat tissues and NSCs, as well as human cells.

Next, we immunoblotted several mitochondrial proteins in Tlk mutant larval brains. As shown in Figures 3E and F, Tlk LoF reduces the amount of NDUFS3, a respiratory chain complex I subunit, and Porin, a voltage-dependent anion channel, in larval brains compared to the control, which was rescued by Tlk Dp. The level of ATP-synthase subunit ATP5α was not changed in the mutant (Figures 3E and F) and was used as an internal control. Combined, our data suggested that Tlk LoF reduces critical mitochondrial proteins in larval brains.

Mitochondrial defects, especially respiratory chain complex deficiencies, are often associated with increased reactive oxygen species (ROS) levels. Impaired respiratory function can cause mitochondria to produce additional ROS, and excessive ROS can oxidize Fe-S centers in NDUFS3 and other Fe-S containing proteins, thereby disrupting mitochondrial function. To test whether Tlk LoF causes excessive ROS, we stained mutant larval brains with an ROS probe, dihydroethidium (DHE). As shown in

Figures 3G and H, mutant NSCs exhibited increased DHE levels compared to the control, which was suppressed by Tlk Dp, suggesting excessive ROS. These data were also supported by our 2,2'-Azino-bis (3-ethylbenzothiazoline-6-sulfonic acid) (ABTS) assays that indirectly assess ROS (Figure S3C). Combined, our data suggest that Tlk LoF disrupts mitochondria and causes excessive ROS.

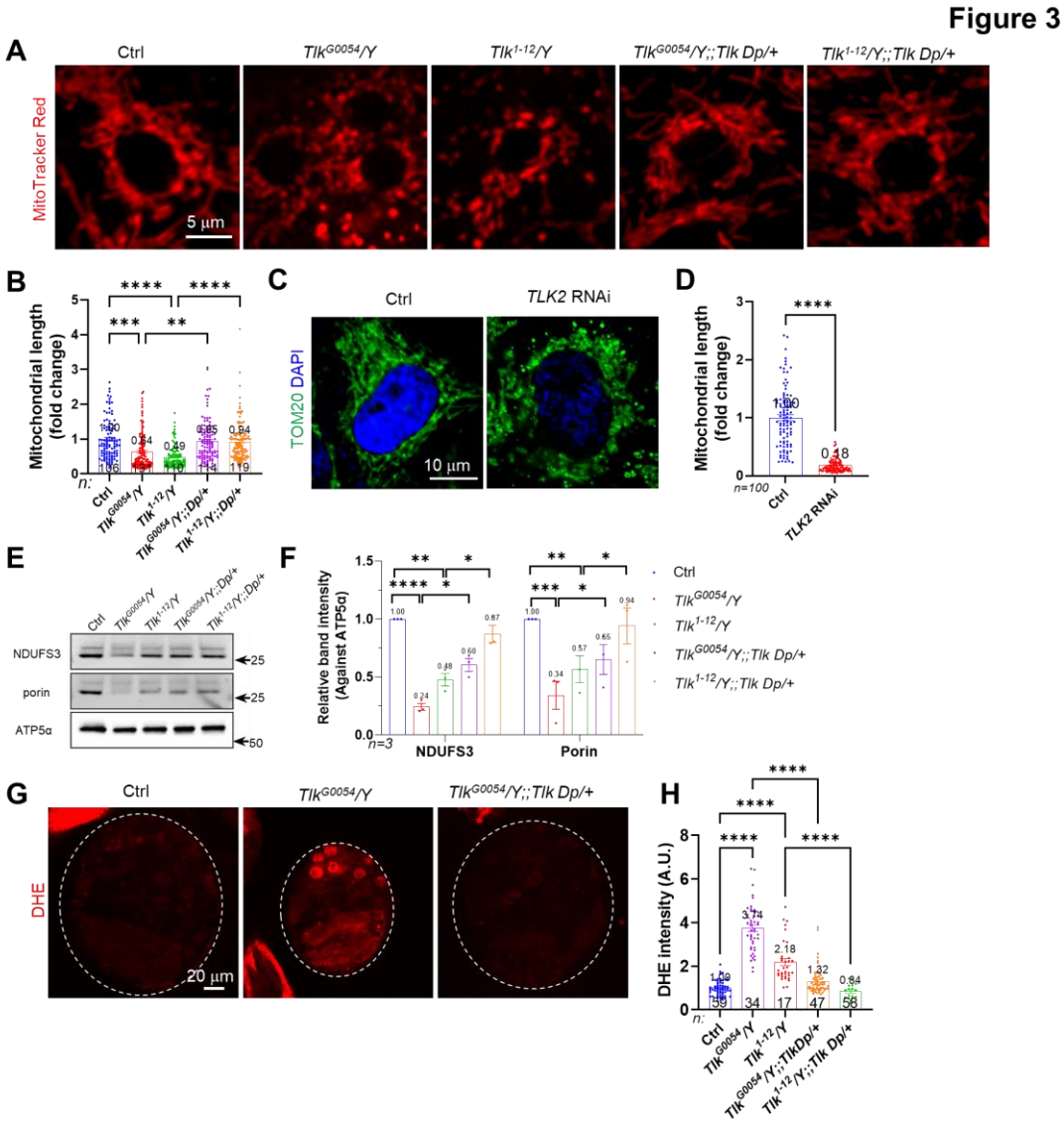

Figure 3. Tlk LoF disrupts mitochondria and causes oxidative stress

(A) NSCs of control (Ctrl), *Tlk* mutant, and rescue larvae stained with MitoTracker Red. Mitochondrial length quantified in B. (C) HeLa cells co-stained with TOM20 (green) and DNA (blue). Mitochondrial morphology quantified in D. (E) Western blots of

NDUFS3, Actin, Porin, and ATP5α in brain extract of third instar larvae, quantified in F. (G) Third instar larval brain lobes stained with DHE, quantified in H. Mean ± SEM. Student's *t*-test (D), one-way ANOVA with Tukey's tests (B, E, and H). **p* < 0.05, ***p* < 0.01, ****p* < 0.001, *****p* < 0.0001.

Figure S3

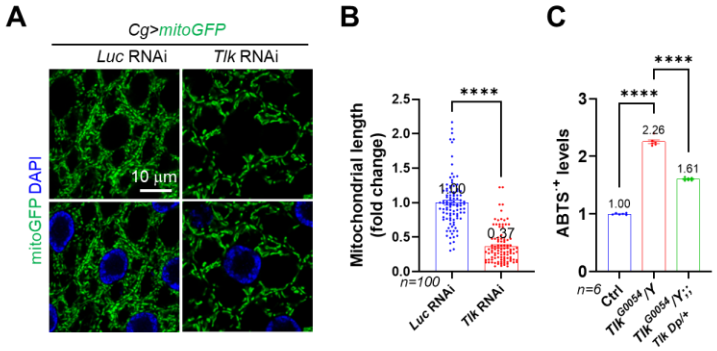

Figure S3. Tlk LoF disrupts mitochondrial morphology

(A) Third instar fat tissues co-expressing a mitochondrially localized GFP (mitoGFP), together with luciferase or Tlk RNAi under the control of Cg-GAL4. The mitochondrial length was quantified in B. (C) Fly larval brains were analyzed using the ABTS assay to assess their ROS levels. Mean ± SEM. Student's *t*-test (B) and one-way ANOVA with Dunnett's tests (C). *****p* < 0.0001.

Tlk LoF suppresses Nrf2-mediated antioxidative responses

Given that antioxidative genes, such as *superoxide dismutase 1* (*Sod1*), *superoxide dismutase 2* (*Sod2*), and *catalase* (*Cat*), are critical ROS regulators, we assessed their expression in Tlk mutant flies. As shown in Figure 4A, the Tlk^{G0054} mutant brain exhibited reduced mRNA levels of *Sod1/2* and *Cat*, which were all restored by Tlk Dp. Notably, the mRNA amounts of several genes encoding mitochondrial proteins, including *NDUFS3*, *Porin*, *SdhA* (encoding a complex II subunit), and *CoVa* (encoding a complex IV subunit), as well as *srl* and *Delg*, key regulators of mitochondrial biogenesis, were unchanged (Figure 4A), suggesting that mitochondrial biogenesis is not affected. We also observed decreased mRNA amounts of *Sod1/2* and *Cat* in the Tlk^{1-12} mutant brain (Figure S4). Combined, these data suggested that Tlk LoF represses antioxidative genes.

Antioxidative genes, including *Sod1/2* and *Cat*, are transactivated by Nrf2, a critical regulator of antioxidative responses. Normally, Nrf2 interacts with Kelch-like ECH-associated protein 1 (Keap1), which promotes its proteasomal degradation. Under oxidative stress, Nrf2 dissociates from Keap1, enters the nucleus, and transactivates antioxidative genes (Suzuki, Otsuki et al. 2016). We show that *Nrf2* mRNA is downregulated in Tlk mutant brains (Figures 4A and S4), which is restored by Tlk Dp. Combined, these data suggest that Tlk LoF represses Nrf2 and its downstream antioxidative genes.

Previously, a heterozygous Keap1 LoF mutant was shown to promote Nrf2 function by reducing Nrf2 degradation (Au, Miller-Fleming et al. 2024). We tested whether it suppresses neural defects caused by Tlk LoF. As shown in Figure 4B, $Keap1^{+/-}$ partially restored *Sod1/2* and *Cat* mRNA amounts. In addition, it reduced brain DHE levels (Figures 4C and D), partially restored aPKC and Mira localization in NSCs (Figures 4E and F), increased the brain size (Figures 4G and H), and suppressed pupal

lethality (Figure 4I), suggesting that activating Nrf2 suppressed ROS and neurodevelopmental defects caused by Tlk LoF.

Figure 4

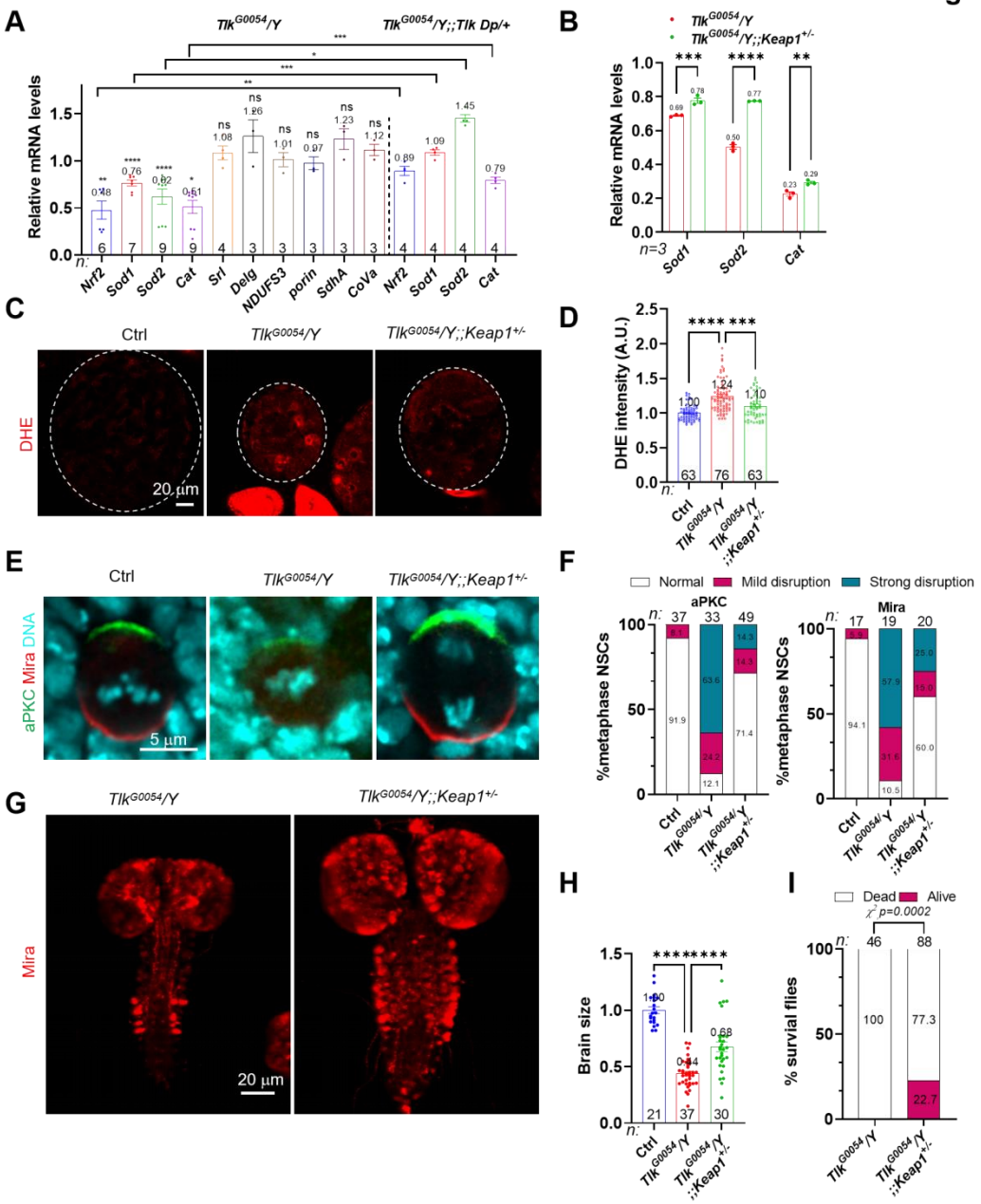

Figure 4. Tlk LoF suppresses Nrf2-mediated antioxidative responses

(A) RT-qPCR data of *Tlk* mutant and rescue larval brains, normalized to the control. (B) RT-qPCR data of larval brains of *Tlk* mutant with or without a heterozygous loss of *Keap1* (*Keap1*$^{+/-}$), normalized to the control. (C) Third instar larval brains stained with

DHE. Ctrl, control. DHE intensities were quantified in D. (E) Metaphase NSCs co-stained with aPKC (green), Mira (red), and DNA (cyan), quantified in F. (G) Central nervous systems of third instar larvae were stained with Mira (red). Brain sizes were quantified in H. (I) Rates of flies survived to adulthood. Mean ± SEM. Student's *t*-tests (A and B) and One-way ANOVA with Dunnett's tests (A, D, and H), and $\chi 2$-tests (I). ns, not significant. *$p < 0.05$, **$p < 0.01$, ***$p < 0.001$, ****$p < 0.0001$.

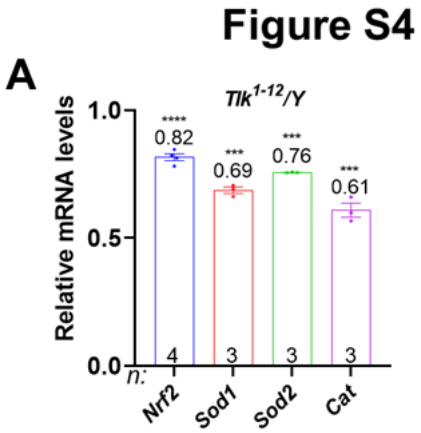

Figure S4. The *Tlk*$^{1-12}$ mutant repressed antioxidative genes

RT-qPCR data of *Tlk*$^{1-12}$ mutant larval brains, normalized against the control. Mean ± SEM. Student's *t*-tests. ***$p < 0.001$, ****$p < 0.0001$.

Tlk regulates Nrf2 via ATF4

Next, we investigated how Tlk LoF represses *Nrf2*. In cancer cells, TLK2 interacts with ATF4 and positively regulates the ATF4 protein level (Wang, Li et al. 2023). Furthermore, ATF4 is a transcriptional factor that transactivates *Nrf2* upon cellular stress (Wang, Chen et al. 2015, Sarcinelli, Dragic et al. 2020). Thus, TLK2/Tlk may regulate Nrf2 via ATF4.

To test this hypothesis, we co-stained Tlk LoF larval brains with ATF4 and Nrf2 antibodies. As shown in Figure S5A, the fluorescent intensities of ATF4 and Nrf2 positively correlated with each other in NSCs. Furthermore, they were both decreased in Tlk mutant NSCs, compared to the control, and restored by Tlk Dp (Figures 5A-C). However, unlike *Nrf2*, *ATF4* mRNA is not downregulated in Tlk mutant brains (Figure S5B). To confirm that ATF4 mediates Tlk-LoF-caused Nrf2 loss, we upregulated ATF4 using an ATF4-containing genomic construct (ATF4 Dp), which increased the *ATF4* mRNA level by ~70% (Figure S5B). As shown in Figures 5D-F, ATF4 Dp partially restored both the mRNA and protein levels of Nrf2 in Tlk mutant brains.

Next, we tested whether ATF4 Dp suppresses neural defects caused by Tlk LoF. As shown in Figure 5G-M, it reduced DHE levels (Figures 5G and H), partially restored aPKC and Mira localization in NSCs (Figures 5I and J), increased the brain size (Figures 5K and L), and suppressed pupal lethality (Figure 5M) in Tlk mutant flies. Combined, our data suggested that Tlk LoF causes elevated ROS and neurodevelopmental defects via downregulating the ATF4-Nrf2 antioxidative axis.

Figure 5

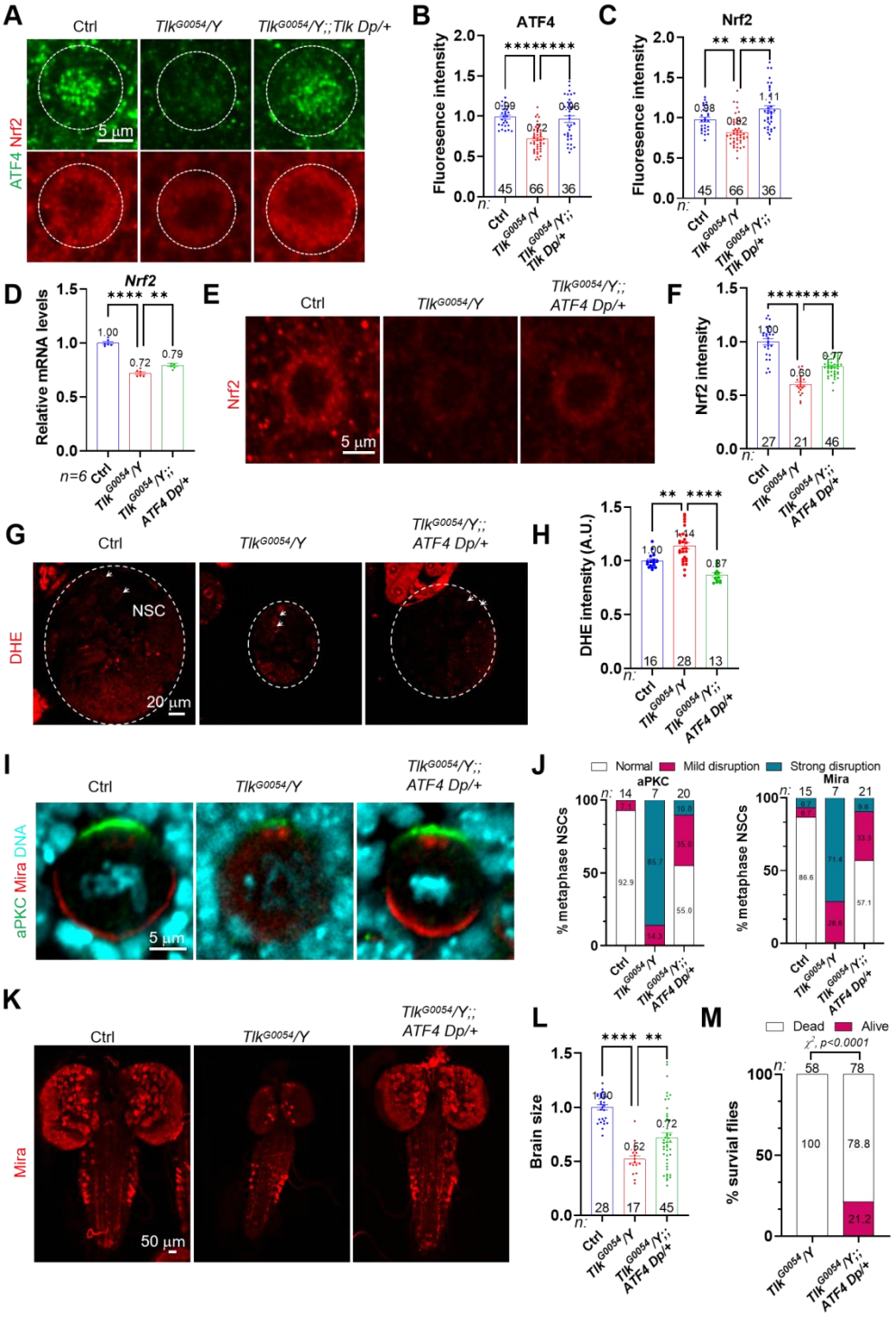

Figure 5. Tlk promotes Nrf2 expression via ATF4 during neurodevelopment

(A) Larval NSCs were co-stained with ATF4 (green) and Nrf2 (red). Ctrl, control. Fluorescent intensities were quantified in B and C. (D) RT-qPCR data of *Nrf2* mRNA in larval brains of Ctrl and *Tlk*^{G0054}*/Y* with or without ATF4 Dp. (E) Larval NSCs were

stained with Nrf2 (red), quantified in F. (G) Larval brain lobes stained with DHE, quantified in (H). (I) Metaphase NSCs co-stained with aPKC (green), Mira (red), and DNA (cyan), quantified in J. (K) Larval brains stained with Mira (red). Brain sizes were quantified in L. (M) Rates of flies survived to adulthood. Mean ± SEM. χ2-tests (M) and one-way ANOVA with Dunnett's tests (all others). $^{**}p < 0.01$, $^{****}p < 0.0001$.

Figure S5

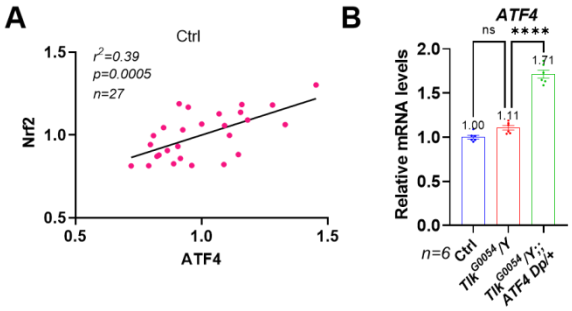

Figure S5. Tlk promotes Nrf2 expression via ATF4

(A) Correlation analyses of ATF4 and Nrf2 intensities. Ctrl, control. (B) RT-PCR results of *ATF4* mRNA in larval brains of Ctrl and Tlk^{G0054}/Y with or without ATF4 Dp. Mean ± SEM. One-way ANOVA with Dunnett's tests, ns, not significant, $^{****}p < 0.0001$.

TLK2 LoF downregulates ATF4 and Nrf2 and causes microcephaly in brain organoids

To verify our findings in human-related models, we first generated human SH-SY5Y neuroblastoma cells stably expressing *TLK2* shRNA, which reduced *TLK2* mRNA by ~60% compared with the control (Figure S6A). Notably, these cells exhibited reduced mRNA levels of *NRF2*, *SOD1/2,* and *CAT*, suggesting that TLK2 promotes Nrf2 function in both fly and human.

Next, we generated brain organoid models of MRD57. First, we generated induced pluripotent stem cells (iPSCs) derived from a male MRD57 patient with a heterozygous *de novo* TLK2 variant (NM_006852.6: c.1015 C>T) (Li, Jiang et al. 2024) and confirmed its variant (Figures S6B), pluripotency, and chromosomal stability (Figures S6C and D). After that, we developed these iPSCs into forebrain organoids in three-dimensional culture using a protocol recapitulating the four stages of brain development (Figure 6A). We observed that the patient-derived brain organoids are smaller compared to parent controls (Figures 6B and C), suggesting microcephaly. Furthermore, seven days after iPSC induction, *NRF2* and *SOD2* were downregulated in patient-derived organoids compared to both parents, and *SOD1* and *CAT* were downregulated compared to one parental control. Agreeing with these data, the ROS indicator 4-hydroxy-nonenal (4-HNE) is upregulated in patient brain organoids (Figures 6E and F). Interestingly, the *ATF4* mRNA level is also reduced in these organoids compared to the parent controls (Figure 6D). In summary, our data suggested that TLK2 LoF suppressed *ATF4*, *Nrf2*, and their downstream antioxidative response genes, leading to excessive ROS and microcephaly in patient-derived brain organoids.

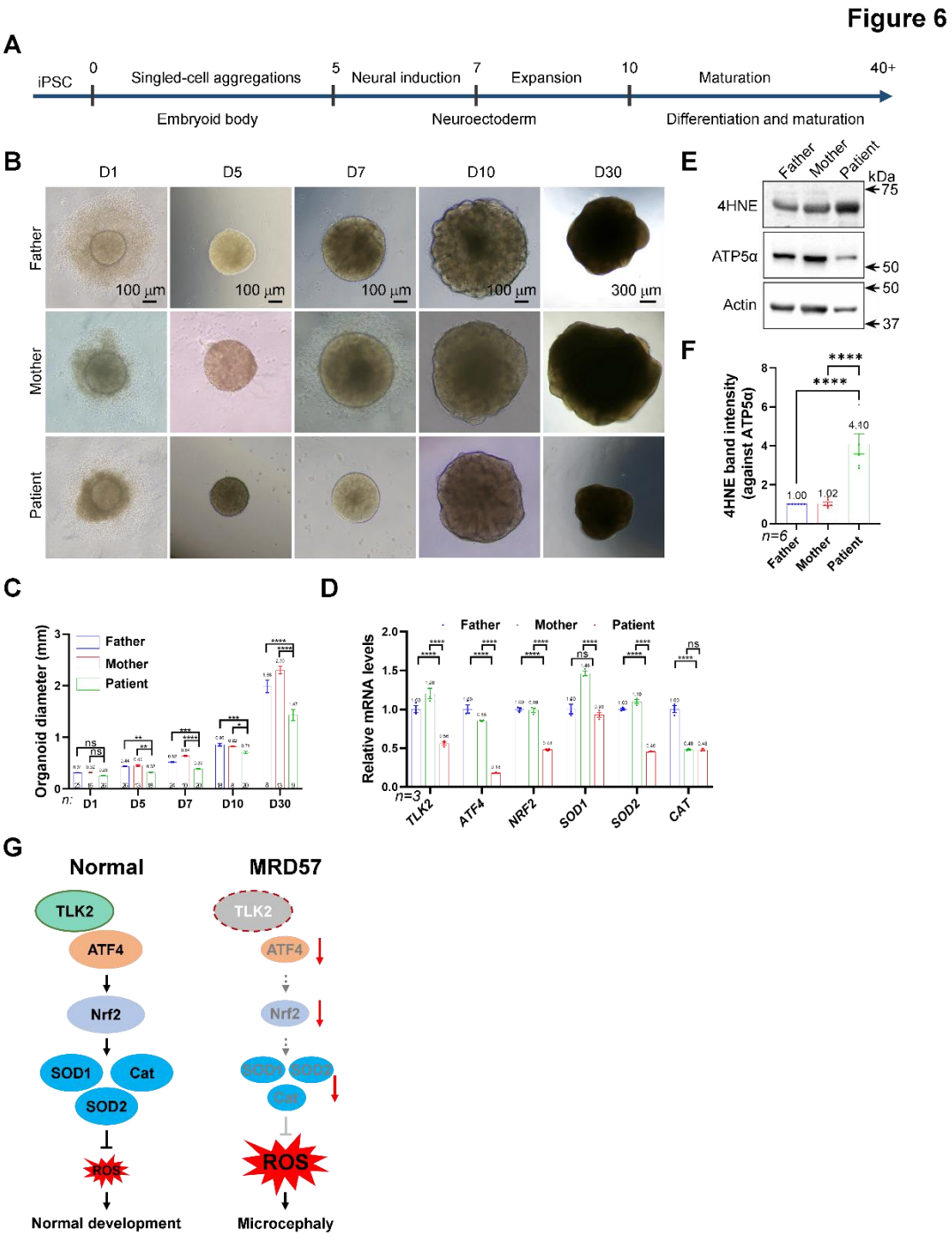

Figure 6. TLK2 regulates NRF2-mediated antioxidative responses in patient brain organoids

(A) A protocol to generate human brain organoids. Stage 1: the embryoid body (EB) stage (day 1-5), when single cells aggregate and early differentiation begins. Stage 2: the induction stage (day 5-7), when the neuroepithelium emerges. Stage 3: the

expansion stage (day 7-10), when the neuroepithelium expands to exhibit a budding morphology. Stage 4: the maturation stage (day 10 and beyond), when nerve cells differentiate and mature. (B) Images of organoids derived from father (top) and patient (bottom) iPSCs at different days. Organoid sizes were quantified in C. (D) mRNA amounts in the organoids at Day 7, measured by RT-qPCR. (E) Western blots, quantified in F. (G) A working model. Left: under normal conditions, ATF4 promotes Nrf2 and downstream antioxidative proteins (e.g., SOD1/2 and catalase), which suppress ROS, causing normal development. Right: in MRD57 pathogenesis, TLK2 LoF reduces ATF4, Nrf2, and their downstream antioxidative proteins, elevates ROS, and causes microcephaly. Mean ± SEM. One-way ANOVA with Dunnett's (F), two-way ANOVA with Dunnett's (C and D), ns, not significant, *$p < 0.05$, **$p < 0.01$, ***$p < 0.001$, ****$p < 0.0001$.

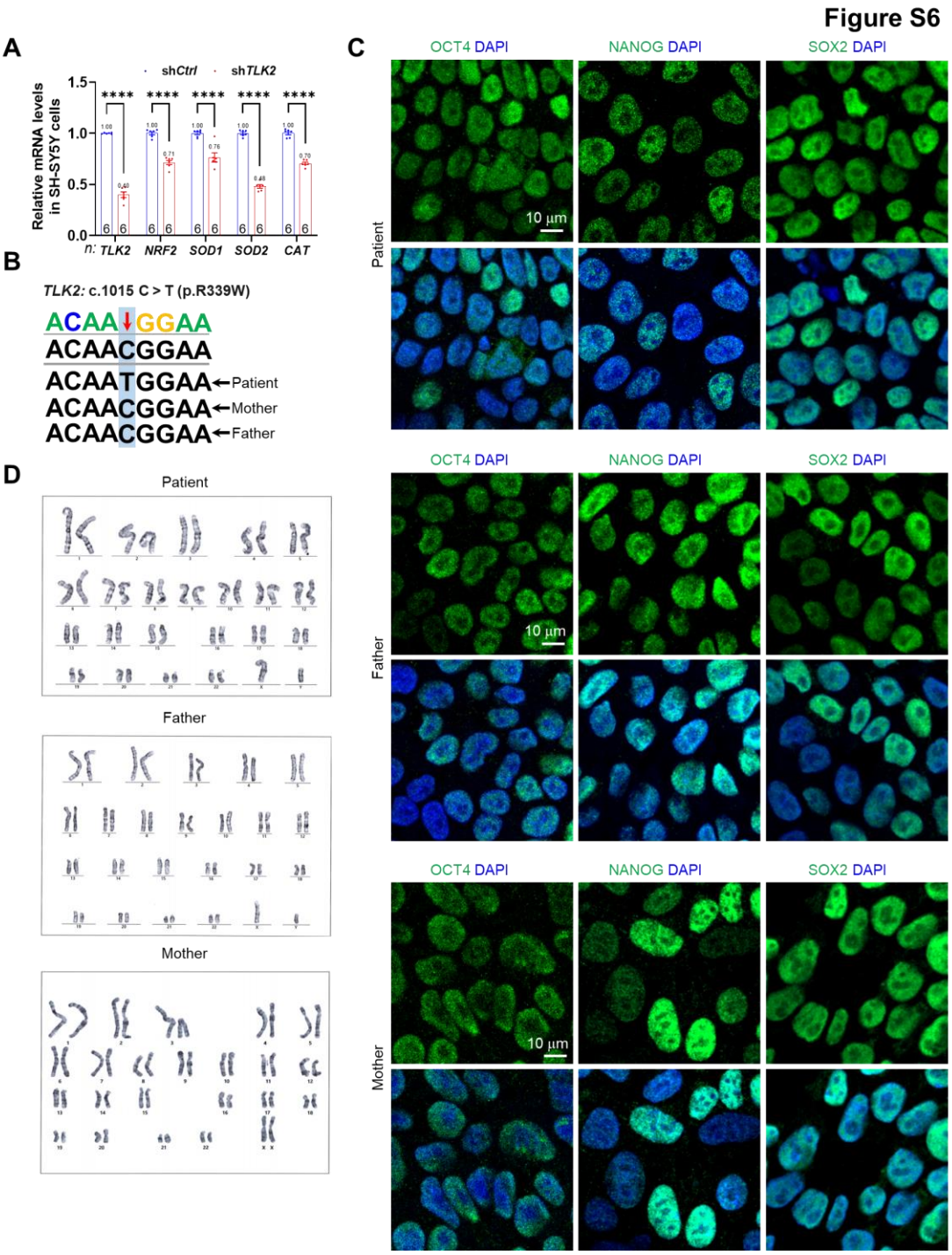

Figure S6. Mutations in the TLK2 and generation of PBMC-derived iPSCs

(A) RT-qPCR data in SH-SY5Y cells expressing shRNA of control (*Ctrl*) or *TLK2*. (B) Alignment of Sanger sequencing data in iPSCs. (C) IPSCs co-stained with the pluripotency markers OCT4, NANOG, and SOX2 (green), together with DAPI (blue). (D) Karyotyping of iPSCs.

Discussion

How TLK2 haploinsufficiency causes MRD57 is unclear. Our study showed that TLK2/Tlk LoF reduced ATF4/Nrf2-mediated antioxidative responses, causing oxidative stress and NPC defects. Thus, these studies delineated the first pathogenic axis and suggested a potential therapeutic target for MRD57.

ATF4 is a stress-activated protein. Upon ER stress, eIF2α is phosphorylated, which represses global translation but promotes ATF4 translation. After entering the nucleus, ATF4 transactivates many stress response genes, including Nrf2. TLK2 could regulate ATF4 abundance via two mechanisms. First, TLK2 colocalizes and interacts with ATF4 in the nucleus (Wang, Li et al. 2023), suggesting posttranslational regulation. Alternatively, TLK2 may upregulate ATF4 translation by promoting eIF2α phosphorylation. Consistent with this idea, genome-wide RNAi screens identified TLK2 RNAi to suppress arsenite-induced stress granule formation, a process that also requires eIF2α phosphorylation (Ohn, Kedersha et al. 2008, Yang, Mathieu et al. 2020).

TLK2 is an evolutionarily conserved kinase with several substrates identified, such as histone chaperone anti-silencing factor 1 (Asf1) (Klimovskaia, Young et al. 2014). Notably, TLK2 gain-of-function (GoF) is also toxic, as TLK2 upregulation was implicated in several types of cancers (Kim, Tan et al. 2016, Wang, Li et al. 2023, He, Xu et al. 2024). Also, overexpressing TLK2 causes cytotoxicity in the *Drosophila* nervous system, which is suppressed by Asf1 RNAi, suggesting that Asf1 contributes to the toxicity of TLK2 GoF (Zhang, Cai et al. 2016).

ROS plays a critical role in many neurological disorders, and drugs with antioxidative effects have been successfully used to treat some of them, such as mitochondrial encephalopathy, amyotrophic lateral sclerosis, etc. (Yoshino 2019, Omata, Aoyama et al. 2024, Pilotto, Chellapandi et al. 2024). Our data suggested that ROS may also contribute to MRD57 pathogenesis, suggesting the potential benefits of

these drugs for MRD57.

MATERIALS AND METHODS

Fly stocks and genetics

Flies were raised and maintained on yeast-cornmeal-syrup food at 25°C. Stocks and crosses were transferred to new vials regularly. The following fly strains were used: *Tlk*$^{1\text{-}12}$*/FM7c, Kr-GAL4, UAS-GFP* (generated in this paper), *Tlk*^{G0054}*/FM7c* (BDSC#11593), *Canton-S*, *Tlk* RNAi #1 (BDSC#33983), *Tlk* RNAi #2 (BDSC#36102), *Luciferase* RNAi (BDSC#31603), *insc*-GAl4 (BDSC#8751), *Keap1*$^{CR01448\text{-}TG4.2}$*/TM3, Sb, Ser* (BDSC#86395), *Tlk* Dp (BDSC#30243), *Cg*-GAL4 (BDSC#7011), *UAS-mito-HA-GFP* (BDSC#8442), and *ATF4* Dp (BDSC#90599).

Generation of CRISPR/Cas9 KO flies

The Tlk sgRNA stock was generated in the laboratory. To generate the Tlk knockout mutant, the Tlk sgRNA stock was crossed with the germline-specific Nos-Cas9 stock. F1 Males carrying both Nos-Cas9 and Tlk sgRNA were crossed with the balancer stocks. Virgin F2 females were collected and crossed individually with balancer stocks to establish the mutant stocks. Once the offspring started to emerge, the genomic DNA of F2 females was isolated, and the DNA fragment of the targeting area was amplified by PCR and sequenced to identify potential mutants. The oligonucleotides used were: TLK2 sense CCACUUAAUAGUGAGUCUUTT and antisense AAGACUCACUAUUAAGUGGTT.

Immunofluorescent staining

Drosophila larvae were dissected in ice-cold PBS, and brains were fixed in 4% EM-grade formaldehyde in the PBX buffer (PBS + 0.3% Triton X-100) for 22 min. The

samples were processed for immunostaining as previously described (Deng, Wang et al. 2022). Images were acquired on an Olympus FV3000 confocal laser scanning microscope using a 40X 0.95 NA or 60X 1.5 NA oil objective. The brightness and contrast of the images obtained were adjusted using Fiji (ImageJ). Confocal imaging of the whole brain was performed by maintaining the same PMT voltage, offset, and laser power settings for the replicate samples in each case. Larval brain images were displayed as projections of 2.5 μm serial Z sections and represent whole compressed Z-stacks of the larval brains.

The fat bodies dissected from 96-h-old larvae were incubated in 4% PFA (Sigma–Aldrich, 158127) for 20 min at room temperature. After being washed three times with 1x PBS, the samples were mounted in 80% glycerol (Sangon Biotech, A100854) containing 5 ng/μL DAPI (Invitrogen, D−1306) and imaged using an LSM880 confocal microscope (Carl Zeiss, Oberkochen, Germany). The cells were fixed in 4% PFA for 20 min at room temperature. Subsequently, samples were permeabilized with PBST (PBS with 0.1% Triton X-100 [Sangon Biotech, T0694]) for 30 min, followed by incubation with primary antibodies for 3 h at room temperature. After washing three times with PBST, the samples were incubated with secondary antibodies for 1 h at room temperature in the dark. Nuclei were stained with 5 ng/μL DAPI for 5 min. Finally, the samples were washed with PBS three times and mounted in 80% glycerol for imaging under an LSM880 confocal microscope.

The primary antibodies used were: rat anti-Dpn (1:500, Abcam, Cat#: ab195172), guinea pig anti-Dpn (1:1000, X.H Yang), rabbit anti-Par6 (1:1000, X.H Yang), rabbit anti-Baz (1:500, X.H Yang), rat anti-Mira (1:500，Abcam, Cat#: ab197788), mouse anti-aPKCζ (H-1) (1:500; Santa Cruz Biotechnology, Cat#: sc-17781), mouse anti-gamma-Tubulin (1:200, Sigma, Cat#: T5326)mouse anti-ATF4 (1:200, Santa Cruz Biotechnology, Cat#: sc-390063), rabbit anti-Nrf2 (1:200, Proteintech, Cat#: 80593-1-RR), mouse anti-TOM20 (1:100, Santa Cruz Biotechnology, sc-17764), Rabbit anti-

Oct-4A (C30A3) (1:300, Cell signaling, Cat#: 2840T), mouse anti-Nanog (1E6C4) (1:300, Santa Cruz Biotechnology, Cat#: sc-293121), and mouse anti-SOX2 (1:300, Santa Cruz Biotechnology, Cat#: sc-365823). The secondary antibodies were conjugated with Alexa Fluor 488, 555, or 647 (ThermoFisher or Jackson Laboratory).

Molecular cloning

The plasmid pCFD5_w-Tlk sgRNA was generated by cloning the sgRNA of Tlk (GATGTCAATGATATGCTGAG) into the pCFD5_w vector (Port and Bullock 2016).

Mitochondria live fluorescent staining

Larval brains were dissected in Schneider's *Drosophila* (SD) medium, immediately incubated in SD medium containing either 50 nM MitoTracker Red CMXRos (Beyotime, Cat#: C1035) or 50 μM dihydroethidium (Beyotime, Cat#: S0063) for 15 minutes, and washed twice in SD. After that, samples were immediately visualized on an Olympus FV3000 confocal laser scanning microscope using a 40X 0.95 NA objective under the same PMT voltage, offset, and laser power settings for the replicate samples in each case.

Western blot

The third instar larval brains or cells were homogenized in the radioimmunoprecipitation assay (RIPA) buffer (50 mM Tris-HCl, pH 7.5, 150 mM NaCl, 1 mM EDTA, 1% Triton X-100, 0.5% sodium deoxycholate, 0.1% SDS, with the cOmplete protease inhibitor from Roch®). Proteins were separated on an SDS-PAGE, and Western blots were performed. The primary antibodies used were: mouse anti-NDUFS3 (1:1,000, Abcam, Cat#: ab14711), mouse anti-Porin (1:500, Abcam, Cat#: ab14734), mouse anti-ATP5α (1:5,000, Abcam, Cat#: ab14748), rabbit anti-Tlk (1:1000, Jenn-Yah Yu), mouse anti-Actin (1:5000, EMD Millipore Corp, Cat#: MAB1501), and rabbit anti-4-Hydroxynonenal (4-HNE) (1:1,000, Abcam, Cat#: ab46545).

mRNA extraction and RT-qPCR

Total mRNA was extracted from cells or tissues using the TRIzol Reagent (TaKaRa, Cat#: 9109) according to the manufacturer's instructions, and reverse transcription (RT) was performed using the iScript cDNA Synthesis Kit (Bio-Rad, Cat#: 1725035BUN). RT-qPCR was performed according to the manufacturer's instructions (iTaq Universal SYBR Green, Bio-Rad, Cat#: 1725120). Reference gene *RPL32/Rpl32* (*ribosomal protein L32*) was used as an internal control. Primers used for RT-qPCR are listed in Table S1.

Cultured cells

All cells were maintained at 37°C in humidified incubators supplemented with 5% CO_2 and were tested monthly for the absence of mycoplasma.

HeLa and SH-SY5Y neuroblastoma cells were cultured in DMEM supplemented with fetal bovine serum and penicillin/streptomycin. SH-SY5Y cells stably expressing control and *TLK2* shRNAs were generated using standard procedures. Briefly, cells were transfected with shRNA constructs containing puromycin resistance and were cultured in media containing 2 μg/mL puromycin for two weeks. Knock-down efficiency was assessed using RT-qPCR.

IPSCs were generated as previously described (Gao, Wang et al. 2022). Briefly, peripheral blood mononuclear cells (PBMCs) were isolated from the whole blood using the PBMC isolation kit (Solarbio P8610) and cultured in StemSpan™-XF (STEMCELL Technologies) with StemSpan™ CC100 (STEMCELL Technologies). After that, PBMCs were seeded onto a 2 × Matrigel-coated 6-well plate, cultured in ReproTeSR™ basial medium (STEMCELL Technologies) supplemented with StemSpan™ CC100 (STEMCELL Technologies), and transfected with plasmids expressing reprogramming factors OCT3/4, SOX2, KLF4, L-MYC, and LIN28 using the Lonza Nucleofector 4D

with program EO-150. After reprogramming, six clones were selected for pluripotency validation and karyotyping.

Forebrain organoid generation

Generation of forebrain organoids from iPSCs was performed according to the manufacturer's instructions (STEMdiff™ Cerebral Organoid Kit, Cat#: 08570). Briefly, iPSC colonies were detached using ReLeSR (STEMCELL, Cat#100-0484) and GCDR (STEMCELL, Cat#100-0485) after passage 2. On Day 0, 9,000 iPSCs were seeded into 100 µL embryoid body formation medium supplemented with 1 µM Y-27632 on an ultra-low attachment 96-well plate (Corning Costar). On Day 5, embryoid bodies were transferred into 100 µL neural induction medium. On Day 7, 20-24 organoids were embedded in hESC-Qualified Matrigel (Corning, Cat#: 354277) and cultured in 1.5 mL expansion medium. On Day 10, embedded organoids were mechanically dissociated from Matrigel by manual pipetting and transferred into an ultra-low attachment 24-well plate (Corning Costar) containing 500 µL maturation medium (Neurobasal medium, DMEM/F12, GlutaMax, N2 and B27 supplements, penicillin/streptomycin, 2-mercaptoethanol, and 2.5 µg/mL human Insulin). After that, organoids were cultured on an orbital shaker, with half-medium changes every 3-4 days.

Quantification and statistical analysis

Drosophila larval brains (dorsal side up) or organoids were on confocal slides. The confocal single plane or z-stacks were taken from the surface to the deep layers of the larval brains. For each genotype, at least 10 brain lobes or 10 NSCs were imaged, and ImageJ or FV3000 software was used for quantification.

Statistical analyses were conducted using GraphPad Prism 9. Tests used and levels of significance for each experiment were explained in the figure legends.

ACKNOWLEDGEMENT

We are grateful to the patient and the family. We thank the following individuals or entities for reagents or services: Jenn-Yah Yu (National Yang Ming Chiao Tung University) for the Tlk antibody, Bloomington Drosophila Stock Center (NIH P40OD018537), TsingHua Fly Center, and National Drosophila Resource Center of China (NDRCC) for fly stocks, the Biological Sample Repository, the Bio-Imaging Core, and the mass spectrometry core at Shenzhen Bay Laboratory for services. We thank Mingdi Fu, Xiao Li, and Yiqian Zhang for technical support. **Funding**: KZ is supported by the Shenzhen Bay Laboratory start-up grant, National Key Research and Development Program of China 2025YFC3409700, and Guangdong Basic and Applied Basic Research Foundation 2023B1515020109. CT is supported by the National Natural Science Foundation of China 32570807. QD is supported by the Young Scientists Fund of the National Natural Science Foundation of China 32400801.

Ethics approval and consent to participate

The ethics of this study were approved by the ethics committee at Children's Hospital, Zhejiang University School of Medicine, with the reference number 2024-IRB-0085-P-01.

Consent for publication

The patient’s parents have signed consent for publication.

Availability of data and materials

All data generated or analyzed during this study are included in this published article and its supplementary information files.

Competing interests

The authors declare no competing interests.

Authors' contributions

Conception: KZ, CT, and QD; Methodology: QD, FH, XZ, YZ, QZ, TL, and WY; Investigation: QD, FH, XZ, CT, and KZ; Visualization: QD and KZ; Funding acquisition: KZ, QD, and CT; Supervision: KZ; Writing – original draft: KZ and QD; Writing – review & editing: KZ, QD, with the help of all others.

Figure legends

See RESULTS

REFERENCES

Au, W. H., L. Miller-Fleming, A. Sanchez-Martinez, J. A. Lee, M. J. Twyning, H. A. Prag, L. Raik, S. P. Allen, P. J. Shaw, L. Ferraiuolo, H. Mortiboys and A. J. Whitworth (2024). "Activation of the Keap1/Nrf2 pathway suppresses mitochondrial dysfunction, oxidative stress, and motor phenotypes in C9orf72 ALS/FTD models." Life Sci Alliance **7**(9).

Bruinsma, W., J. van den Berg, M. Aprelia and R. H. Medema (2016). "Tousled-like kinase 2 regulates recovery from a DNA damage-induced G2 arrest." EMBO Rep **17**(5): 659-670.

Deng, Q., C. Wang, C. T. Koe, J. P. Heinen, Y. S. Tan, S. Li, C. Gonzalez, W. K. Sung and H. Wang (2022). "Parafibromin governs cell polarity and centrosome assembly in Drosophila neural stem cells." PLoS Biol **20**(10): e3001834.

Doe, C. Q. (2008). "Neural stem cells: balancing self-renewal with differentiation." Development **135**(9): 1575-1587.

Gao, L., F. Wang, Y. Wang, L. Hu and J. Mao (2022). "A protocol for the generation of patient-specific iPSC lines from peripheral blood mononuclear cells." STAR Protoc **3**(3): 101530.

He, T., B. Xu and H. Ma (2024). "TLK2 promotes progression of hepatocellular carcinoma through Wnt/β-catenin signaling." Transl Cancer Res **13**(7): 3729-3741.

Kim, J. A., Y. Tan, X. Wang, X. Cao, J. Veeraraghavan, Y. Liang, D. P. Edwards, S. Huang, X. Pan, K. Li, R. Schiff and X. S. Wang (2016). "Comprehensive functional analysis of the tousled-like kinase 2 frequently amplified in aggressive luminal breast cancers." Nat Commun **7**: 12991.

Klimovskaia, I. M., C. Young, C. B. Strømme, P. Menard, Z. Jasencakova, J. Mejlvang, K. Ask, M. Ploug, M. L. Nielsen, O. N. Jensen and A. Groth (2014). "Tousled-like kinases phosphorylate Asf1 to promote histone supply during DNA replication." Nature Communications **5**(1): 3394.

Lee, S. B., S. Segura-Bayona, M. Villamor-Payà, G. Saredi, M. A. M. Todd, C. S. Attolini, T. Y. Chang, T. H. Stracker and A. Groth (2018). "Tousled-like kinases stabilize replication forks and show synthetic lethality with checkpoint and PARP inhibitors." Sci Adv **4**(8): eaat4985.

Li, H. Y., C. M. Jiang, R. Y. Liu and C. C. Zou (2024). "Report of one case with de novo mutation in TLK2 and literature review." BMC Pediatr **24**(1): 732.

Ohn, T., N. Kedersha, T. Hickman, S. Tisdale and P. Anderson (2008). "A functional RNAi screen links O-GlcNAc modification of ribosomal proteins to stress granule and processing body assembly." Nat. Cell Biol **10**(10): 1224-1231.

Omata, T., H. Aoyama, K. Murayama, M. Takayanagi, R. Kawaguchi, R. Fujimoto and J. I. Takanashi (2024). "Efficacy of a mitochondrial drug cocktail in preventing acute encephalopathy with biphasic seizures and late reduced diffusion." J Neurol Sci **466**: 123245.

Pavinato, L., M. Villamor-Payà, M. Sanchiz-Calvo, C. Andreoli, M. Gay, M. Vilaseca, G. Arauz-Garofalo, A. Ciolfi, A. Bruselles, T. Pippucci, V. Prota, D. Carli, E. Giorgio, F. C. Radio, V. Antona, M. Giuffrè, K. Ranguin, C. Colson, S. De Rubeis, P. Dimartino, J. D. Buxbaum, G. B. Ferrero, M. Tartaglia, S. Martinelli, T. H. Stracker and A. Brusco (2022). "Functional analysis of TLK2 variants and their proximal interactomes implicates impaired kinase activity and chromatin maintenance defects in their pathogenesis." J Med Genet **59**(2): 170-179.

Pilotto, F., D. M. Chellapandi and H. Puccio (2024). "Omaveloxolone: a groundbreaking milestone as the first FDA-approved drug for Friedreich ataxia." Trends Mol Med **30**(2): 117-125.

Port, F. and S. L. Bullock (2016). "Augmenting CRISPR applications in Drosophila with tRNA-flanked sgRNAs." Nature Methods **13**(10): 852-854.

Reijnders, M. R. F., K. A. Miller, M. Alvi, J. A. C. Goos, M. M. Lees, A. de Burca, A. Henderson, A. Kraus, B. Mikat, B. B. A. de Vries, B. Isidor, B. Kerr, C. Marcelis, C. Schluth-Bolard, C. Deshpande, C. A. L. Ruivenkamp, D. Wieczorek, D. Baralle, E. M. Blair, H. Engels, H.-J. Lüdecke, J. Eason, G. W. E. Santen, J. Clayton-Smith, K. Chandler, K. Tatton-Brown, K. Payne, K. Helbig, K. Radtke, K. M. Nugent, K. Cremer, T. M. Strom, L. M. Bird, M. Sinnema, M. Bitner-Glindzicz, M. F. van Dooren, M. Alders, M. Koopmans, L. Brick, M. Kozenko, M. L. Harline, M. Klaassens, M. Steinraths, N. S. Cooper, P. Edery, P. Yap, P. A. Terhal, P. J. van der Spek, P. Lakeman, R. L. Taylor, R. O. Littlejohn, R. Pfundt, S. Mercimek-Andrews, A. P. A. Stegmann, S. G. Kant, S. McLean, S. Joss, S. M. A. Swagemakers, S. Douzgou, S. A. Wall, S. Küry, E. Calpena, N. Koelling, S. J. McGowan, S. R. F. Twigg, I. M. J. Mathijssen, C. Nellaker, H. G. Brunner and A. O. M. Wilkie (2018). "De Novo and Inherited Loss-of-Function Variants in TLK2: Clinical and Genotype-Phenotype Evaluation of a Distinct Neurodevelopmental Disorder." The American Journal of Human Genetics **102**(6): 1195-1203.

Sarcinelli, C., H. Dragic, M. Piecyk, V. Barbet, C. Duret, A. Barthelaix, C. Ferraro-Peyret, J. Fauvre, T. Renno, C. Chaveroux and S. N. Manié (2020). "ATF4-Dependent NRF2 Transcriptional Regulation Promotes Antioxidant Protection during Endoplasmic Reticulum Stress." Cancers (Basel) **12**(3).

Segura-Bayona, S., P. A. Knobel, H. González-Burón, S. A. Youssef, A. Peña-Blanco, É. Coyaud, T. López-Rovira, K. Rein, L. Palenzuela, J. Colombelli, S. Forrow, B. Raught, A. Groth, A. de Bruin and T. H. Stracker (2017). "Differential requirements for Tousled-like kinases 1 and 2 in mammalian development." Cell Death & Differentiation **24**(11): 1872-1885.

Segura-Bayona, S. and T. H. Stracker (2019). "The Tousled-like kinases regulate genome and epigenome stability: implications in development and disease." Cell Mol Life Sci **76**(19): 3827-3841.

Siller, K. H. and C. Q. Doe (2009). "Spindle orientation during asymmetric cell division." Nature Cell Biology **11**(4): 365-374.

Suzuki, M., A. Otsuki, N. Keleku-Lukwete and M. Yamamoto (2016). "Overview of redox regulation by Keap1–Nrf2 system in toxicology and cancer." Current Opinion in Toxicology **1**: 29-36.

Wang, M., J. Li, X. Yang, Q. Yan, H. Wang, X. Xu, Y. Lu, D. Li, Y. Wang, R. Sun, S. Zhang, Y. Zhang, Z. Zhang, F. Meng and Y. Li (2023). "Targeting TLK2 inhibits the progression of gastric cancer by reprogramming amino acid metabolism through the mTOR/ASNS axis." Cancer Gene Therapy **30**(11): 1485-1497.

Wang, S., X. A. Chen, J. Hu, J. K. Jiang, Y. Li, K. Y. Chan-Salis, Y. Gu, G. Chen, C. Thomas, B. F. Pugh and Y. Wang (2015). "ATF4 Gene Network Mediates Cellular Response to the Anticancer PAD Inhibitor YW3-56 in Triple-Negative Breast Cancer Cells." Mol Cancer Ther **14**(4): 877-888.

Yang, P., C. Mathieu, R. M. Kolaitis, P. Zhang, J. Messing, U. Yurtsever, Z. Yang, J. Wu, Y. Li, Q. Pan, J. Yu, E. W. Martin, T. Mittag, H. J. Kim and J. P. Taylor (2020). "G3BP1 Is a Tunable Switch that Triggers Phase Separation to Assemble Stress Granules." Cell **181**(2): 325-345 e328.

Yoshino, H. (2019). "Edaravone for the treatment of amyotrophic lateral sclerosis." Expert Rev Neurother **19**(3): 185-193.

Zhang, Y., R. Cai, R. Zhou, Y. Li and L. Liu (2016). "Tousled-like kinase mediated a new type of cell death pathway in Drosophila." Cell Death & Differentiation **23**(1): 146-157.

Zhou, J., L. Xu, X. Duan, W. Liu, X. Zhao, X. Wang, W. Shang, X. Fang, H. Yang, L. Jia, J. Bai, J. Zhao, L. Wang and C. Tong (2019). "Large-scale RNAi screen identified Dhpr as a regulator of mitochondrial morphology and tissue homeostasis." Sci Adv **5**(9): eaax0365.